Light-emitting organic field-effect transistor using an organic heterostructure within the transistor channel

De Vusser, S.; Schols, S.; Steudel, S.; VERLAAK, Stijn; GENOE, Jan; OOSTERBAAN, Wibren; LUTSEN, Laurence; VANDERZANDE, Dirk & Heremans, P. (2006) Light-emitting organic field-effect transistor using an organic heterostructure within the transistor channel. In: APPLIED PHYSICS LETTERS, 89(22). p. 223504-....

DOI: 10.1063/1.2392937
Handle: http://hdl.handle.net/1942/1460

Light-emitting organic field-effect transistors using an organic heterostructure inside the transistor channel

Stijn De Vusser[a,b], Soeren Steudel[a,b], Sarah Schols[a,b], Stijn Verlaak[a], Jan Genoe[a], Wibren D. Oosterbaan[c], Laurence J. Lutsen[c], Dirk J.M. Vanderzande[c,d], Paul L. Heremans[a,b]

[a] IMEC - MCP/PME, Kapeldreef 75, B-3001 Leuven, Belgium
[b] Katholieke Universiteit Leuven, ESAT/INSYS, Kasteelpark Arenberg 10, B-3001 Leuven, Belgium
[c] IMEC - IMOMEC, Wetenschapspark 1, B-3590 Diepenbeek, Belgium
[d] Hasselt University, IMO, Agoralaan, Building D, B-3590 Diepenbeek, Belgium

ABSTRACT

We have realized a light-emitting organic field-effect transistor (LEOFET). Excitons are generated at the interface of an n-type and a p-type organic semiconductor heterostructure inside the transistor channel. The dimensions and the position of the p-n heterostructure are defined by photolithography. The recombination region is several microns from the metal electrodes. Therefore, the exciton quenching probability in this device is reduced. Numerical simulations show that the recombination region can move within the transistor channel by changing the biasing conditions.

Keywords: Light-emitting organic field-effect transistor (LEOFET)

1. INTRODUCTION

Organic semiconductors have been incorporated in a wide range of devices, including organic thin-film transistors (OTFTs) and circuits, organic solar cells, organic non-volatile memories and organic light-emitting diodes (OLEDs). Display applications are a particularly important driver for the further development of this organic technology. As a matter of fact, many commercially available products nowadays already contain OLED-based displays. The driving backplane circuit of these displays is still based on an inorganic technology, usually amorphous silicon. On lab scale, however, OTFT-based display backplanes have been combined with liquid crystal,[1] E-ink,[2] and OLED[3] display elements.

Light-emitting organic field-effect transistors (LEOFETs) may become an interesting structure in this field, as they combine the optical output of an OLED and the gate control of an OTFT in a single device. Therefore, displays based on LEOFETs may eliminate the difficult integration of the light-emitting structure and the organic driving backplane. Moreover, LEOFETs are interesting devices in order to study the opto-electronical properties of organic semiconductors.

The first LEOFET, using tetracene as the organic semiconductor, was published by Hepp *et al.* in 2003.[4] Ever since, other research groups have published results on tetracene-based LEOFETs, dealing with experimental[5,6] as well as theoretical aspects.[7,8]

This same basic type of LEOFETs, based on one unipolar organic semiconductor, has also been realized using polymers[9,10] and doped small molecules[11] as the organic semiconductor. Electroluminescence in these LEOFETs occurs very close to the electron injecting metal electrode. Therefore, the electron injecting electrode in this type of devices will quench most of the excitons, and absorb the emitted light.[12,13]

Rost *et al.* reported on a LEOFET in which the active layer was formed by a heterostructure of a p-type and an n-type organic semiconductor, either by coevaporation[14] or by subsequent evaporation of both semiconductors.[15] The presence of an n-type and p-type semiconductor is a clear advantage in comparison to

Further author information (send correspondence to S.D.V.):
E-mail: stijn.devusser@imec.be, Telephone: +32 16 281755, Fax: +32 16 281501

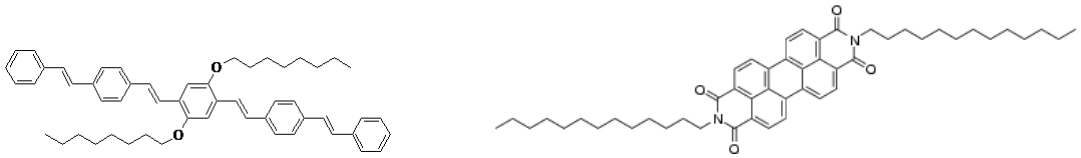

(a) (b)

Figure 1. (a) Structural formula of OOctyl-OPV5 and (b) of PTCDI-$C_{13}H_{27}$.

tetracene-based p-type-only LEOFETs. However, as neither of the semiconductors is patterned, there is little control over the position in the channel where the light is emitted.

Zaumseil *et al.* recently reported on a LEOFET using a single polymeric ambipolar semiconductor.[16] This is the first demonstration of a device in which the light-emitting zone can be spatially controlled. This proves unambiguously that for certain biasing conditions, accumulation layers of both electrons and holes are formed in the ambipolar material. A similar device, showing the same properties, was very recently reported by Swensen *et al.*[17]

In this manuscript, a structure is proposed in which excitons are generated at the interface of an n-type and a p-type semiconductor. However, in contrast to previously published heterostructure LEOFETs, the location and the dimensions of the overlap between the semiconductors are defined by photolithography. Therefore, the recombination zone can be located inside the transistor channel, away from the metal source and drain electrodes.

2. EXPERIMENTAL

Devices were processed on a highly doped n++ Si wafer, acting both as the substrate and the gate electrode. The gate dielectric is a layer of 100 nm thermally grown SiO_2. Source and drain electrodes consist of a layer of 20 nm Au, patterned by optical photolithography and lift-off. On top of this structure, a 5 μm thick layer of photoresist is patterned by optical photolithography. This photoresist profile in fact creates a shadow mask that is integrated with the substrate.

1,4-Bis(octyloxy)-2,5-bis[(*E*)-4-(*E*)-styrylstyryl]benzene (OOctyl-OPV5), an oligo(phenylene vinylene) derivative (HOMO=5.49 eV, LUMO=2.9 eV, as measured by cyclic voltammetry), was used as the p-type semiconductor.[18] Details about the synthesis and analysis are given in Appendix A of this paper. Fig. 1(a) shows the

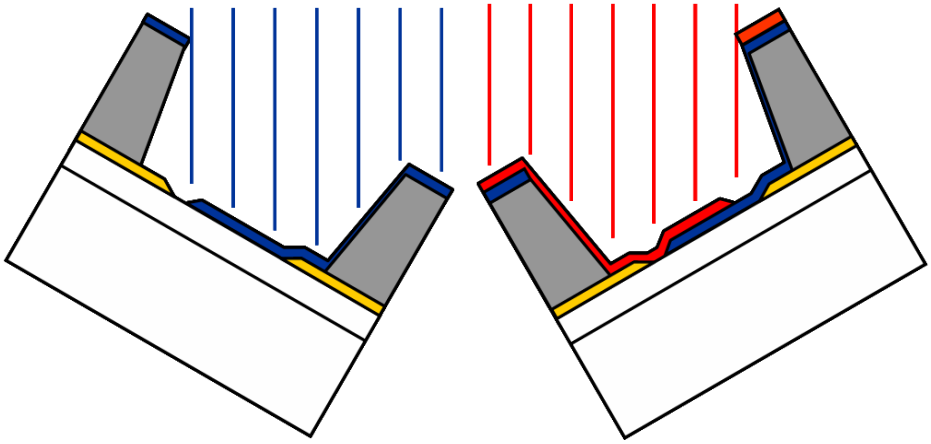

(a) (b)

Figure 2. (a) Schematic illustration of the p-type semiconductor deposition and (b) schematic illustration of the n-type semiconductor deposition.

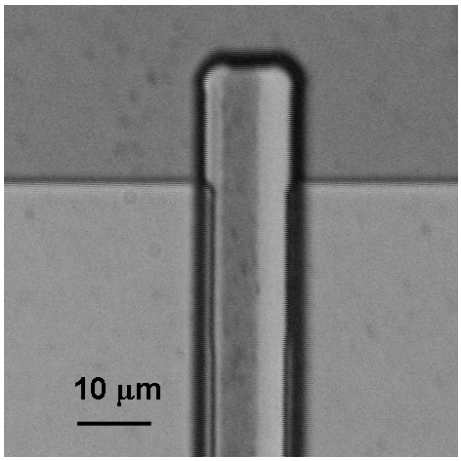

Figure 3. The p-n heterostructure region is well defined inside the transistor channel, and is not in contact with the metal source/drain electrodes.

structural formula of OOctyl-OPV5. After a cleaning step, 50 nm of OOctyl-OPV5 is evaporated in ultra-high vacuum, while the substrate is tilted in a $+45\,^{\circ}$ angle relative to the molecular flux. Because of the tilted deposition through the integrated shadow mask, the p-type semiconductor is covering one metal electrode completely, as well as part of the channel. The remaining part of the channel, as well as the other metal electrode, are in the shadow of the integrated shadow mask during the evaporation, hence no p-type material is deposited there. This is schematically illustrated in Fig. 2(a).

N,*N*'-Ditridecylperylene-3,4,9,10-tetracarboxylic diimide (PTCDI-$C_{13}H_{27}$), a perylene derivative (HOMO=5.4 eV, LUMO=3.4 eV) was used as the n-type semiconductor.[15,19] PTCDI-$C_{13}H_{27}$ was purchased from Aldrich and purified through vacuum sublimation. Fig. 1(b) shows the structural formula of PTCDI-$C_{13}H_{27}$. 50 nm of PTCDI-$C_{13}H_{27}$ is evaporated in ultra-high vacuum, while keeping the substrate in a $-45\,^{\circ}$ angle relative to the flux. Correspondingly, the n-type semiconductor is covering the previously uncovered metal electrode, as well as part of the channel. The other part of the channel, as well as the metal electrode that was already covered by the p-type material, are in the shadow of the shadow mask during the n-type deposition. Fig. 2(b) schematically depicts this deposition.

By carefully defining all dimensional parameters involved in the design and processing of the device, it is possible to create a region inside the channel where the p-type and the n-type material are overlapping. As can be verified in Fig. 3, this region is relatively far (in the order of a few μm) from the metal electrodes. As the exciton diffusion length is typically in the order of 100 nm, this method leads to a reduced exciton quenching probability. The electroluminescence efficiency is obviously favored because of this. The width of the p-n heterostructure, as well as the distance between the metal electrodes and this region, can be freely chosen within certain limits by adjusting the dimensions of the integrated shadow mask.

3. RESULTS

By applying a bias to the gate, source and drain electrodes, electrons and holes can be injected from the source and drain contacts into the organic semiconducting films. In fact, the traditional nomenclature of source and drain is ambiguous in this type of device, since both electrodes do inject carriers in the organic materials. Therefore, we arbitrarily define the source as the electrode that injects holes in the p-type semiconductor. The source is also the electrode that is held at ground potential. The drain is the electron injecting electrode that is in contact with the n-type semiconductor.

The experimentally measured electrical characteristics of the device are shown in Fig. 4(a). The device was measured immediately after the n-type semiconductor deposition in an inert N_2 atmosphere using an Agilent

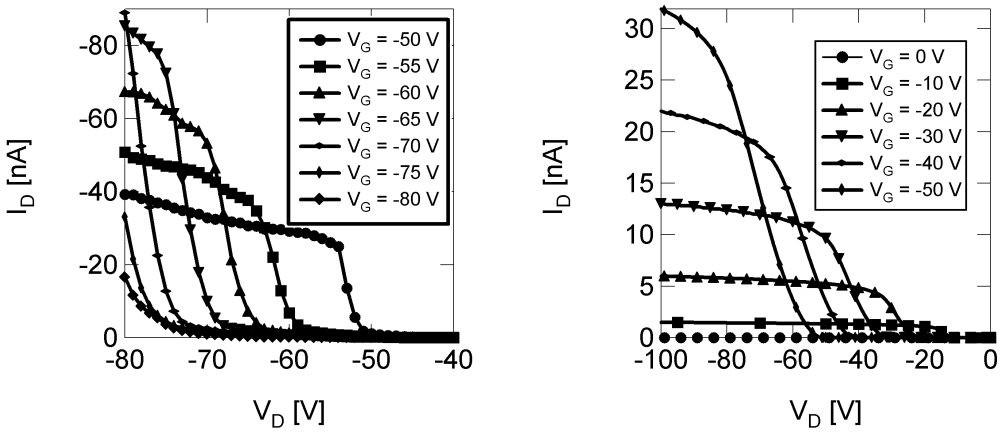

(a) (b)

Figure 4. Electrical characteristics of the device: (a) experimental ($W/L = 200/10$) and (b) simulated ($W/L = 200/10$).

4156C parameter analyzer. Assuming that the threshold voltages of both organic semiconductors are equal to 0 V, the electrical characteristics can be qualitatively explained as follows: for a fixed negative gate voltage V_G, holes are injected from the source into the p-type material, and a hole accumulation layer is formed. For drain voltages $|V_D| < |V_G|$, there is only a very low current, since there is no electron injection in the n-type semiconductor, and the hole mobility in PTCDI-$C_{13}H_{27}$ is low. When $|V_D| \geq |V_G|$, electrons are injected from the drain into the n-type material, forming an electron accumulation layer. The current through the device increases quadratically, as can be expected from the theory of an ambipolar transistor.[20] At a certain drain voltage, the electron current in the n-type material at the p-n interface is equal to the hole current in the p-type material. In contrast to previously published LEOFETs,[15,16,19] increasing $|V_D|$ beyond this voltage leads to a saturation of the current. This is explained by the fact that a further increase of $|V_D|$ does not lead to an increase of the hole current. The electron current, on the other hand, is increased by $|V_D|$, but it is blocked at the p-n interface due to the energy difference between the LUMO of PTCDI-$C_{13}H_{27}$ and that of OOctyl-OPV5.

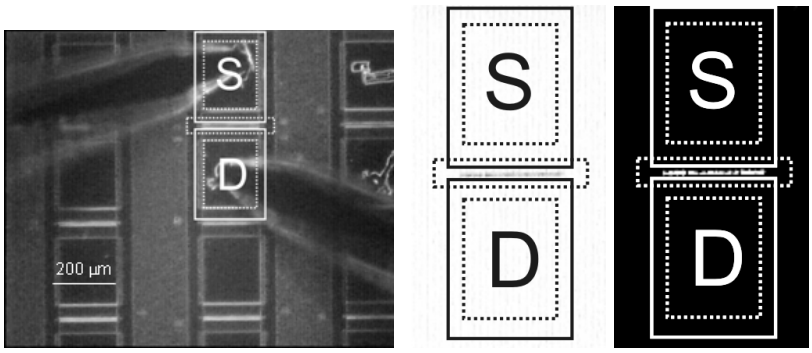

(a) (b) (c)

Figure 5. Optical microscope image of (a) the LEOFET measurement setup (microscope lamp on). The straight lines represent the metal source and drain electrodes. The dotted lines represent the apertures in the integrated shadow mask for the active area and for the contact pads of the source and drain electrodes; (b) an inverse image of the optical output upon bias (microscope lamp off; no image enhancement); (c) an image of the optical output upon bias (microscope lamp off; the image consists of several superimposed images); $W/L = 200/10$.

Table 1. Summary of the material parameters used in the 2D device simulator.

	OOctyl-OPV5	PTCDI-$C_{13}H_{27}$
LUMO (eV)	2.9	3.4
HOMO (eV)	5.45	5.45
μ_e (cm^2/Vs)	$1 \cdot 10^{-6}$	$2 \cdot 10^{-2}$
μ_h (cm^2/Vs)	$5 \cdot 10^{-3}$	$5 \cdot 10^{-4}$

When the biasing conditions are such that the potential at some point in the channel equals the gate potential, the electron and hole accumulation layers meet at this point, and excitonic recombination of electrons and holes occurs. It was indeed experimentally observed that the device emits light upon the radiative decay of the excitons. The intensity of the light clearly increases with the electron and hole current, caused by increasing $|V_G|$. Figs. 5(a) and 5(b) illustrate the measurement setup and the resulting optical output, respectively. For reasons of clarity, the optical output is shown inversely; otherwise, no image manipulation was performed on Fig. 5(b). Fig. 5(c) shows an enhanced version of the same optical output, whereby several images were superimposed.

The experimentally observed behavior is qualitatively confirmed by the simulated characteristics of Fig. 4(b). The device was simulated using the Silvaco Atlas 2D device simulator. The material parameters used in the simulations are summarized in Table 1. Source and drain electrodes are positioned at $x < 1$ μm and $x > 9$ μm, respectively. For the sake of simplicity, the threshold voltage of both materials was assumed to be 0 V, and no interface states were taken into account. Therefore, the quantitative differences between Figs. 4(a) and 4(b) can be explained by the fact that the first-order approximations used in the simulations do not hold in real life.

It is assumed that the light emission zone moves within the transistor channel, exactly as has been previously described by Zaumseil *et al.*[16] Due to the small dimensions of our device and the fact that our measurement setup is not equipped with a microscope with sufficiently high magnification, we have been unsuccesful in demonstrating this experimentally. However, this theory is supported by numerical simulations.

Fig. 6 clearly illustrates that the recombination region moves from right to left (i.e., from the n-region to the p-region) by increasing $|V_D|$ while keeping V_G at a fixed negative value. At $V_D = V_G$, recombination occurs at the gate dielectric-organic interface in the n-type material. Excitons are generated close to the electron injecting drain electrode, which will in practice lead to quenching of the excitons at the metal electrode. The recombination rate and the potential distribution in this situation are depicted in Figs. 6(a) and 7(a), respectively. For these biasing conditions, injected electrons are readily available from the drain; holes are transported from the source electrode through the p-type material, and encounter a negligibly low barrier at the p-n interface. Therefore, the holes can travel through the n-type material (with a lower mobility), and are able to recombine with the electrons in the n-type material.

At higher $|V_D|$, the position where the channel potential equals V_G moves towards the hole-injecting source contact, as shown in Figs. 7(b)-7(d). As a consequence, by increasing $|V_D|$, holes and electrons meet at a position that moves towards the hole injecting source electrode, which is obvious from Figs. 6(b)-6(d).

At a sufficiently high $|V_D|$, the recombination zone is located at the far edge of the n-type material ($x = 3$ μm). Simulated data show that this situation is reached for $V_G = -20$ V and $|V_D| \geq 45$ V. Electrons in the n-type material face a relatively high injection barrier at the interface with the p-type material. Hence, electrons cannot be injected from the n-type into the p-type semiconductor, and the recombination zone does not move towards the source any further. This is also the reason for the experimentally observed saturation of the current in the $I_D - V_D$ measurements. Instead of moving to the source electrode, the recombination zone increases in height when $|V_D|$ is further increased, as shown by the simulations. Figs. 6(e)-6(f) and 7(e)-7(f) show that, indeed, there is virtually no difference between the potential distribution left from the far edge of the n-type material ($x \leq 3$ μm) at $V_D = -45$ V and $V_D = -80$ V (for $V_G = -20$ V). Therefore, the drain current I_D saturates, and the electron-hole recombination region does not move left anymore by a further increase of $|V_D|$.

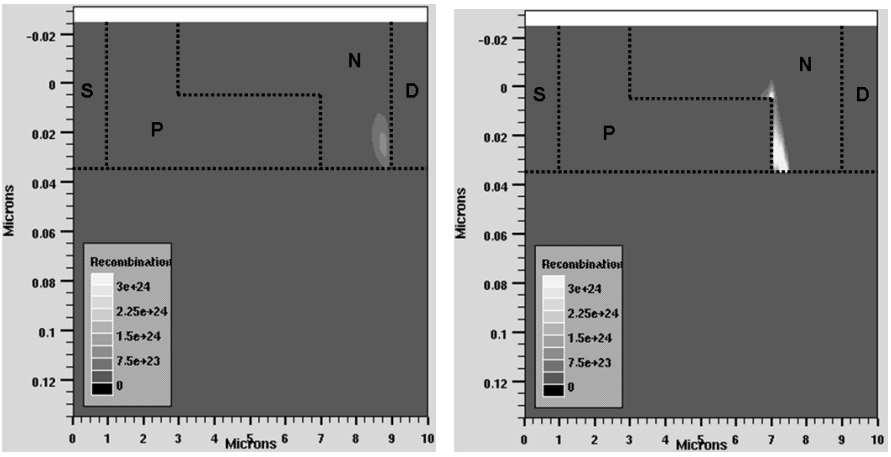

(a) $V_G = -20$ V; $V_D = -20$ V. (b) $V_G = -20$ V; $V_D = -25$ V.

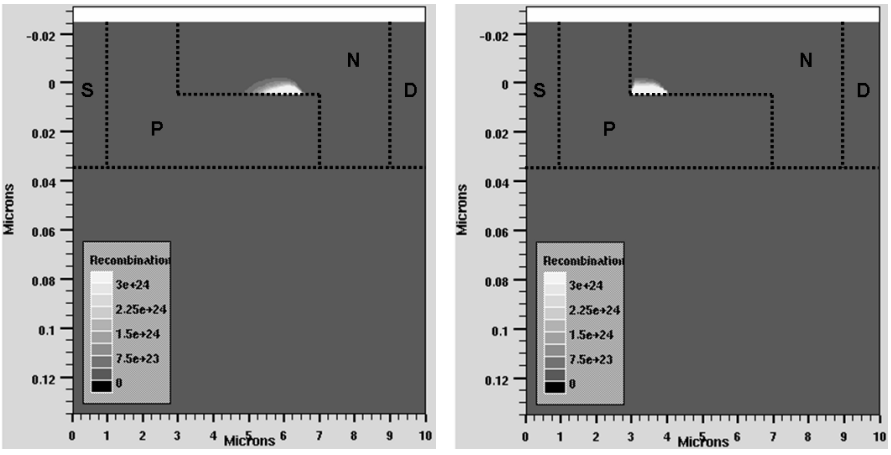

(c) $V_G = -20$ V; $V_D = -30$ V. (d) $V_G = -20$ V; $V_D = -40$ V.

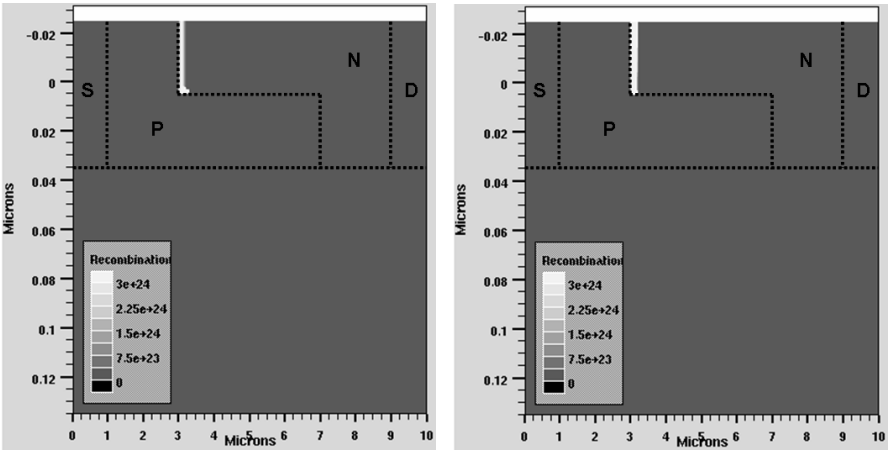

(e) $V_G = -20$ V; $V_D = -45$ V. (f) $V_G = -20$ V; $V_D = -80$ V.

Figure 6. Numerical simulations indicate that the recombination zone moves within the transistor channel by increasing $|V_D|$.

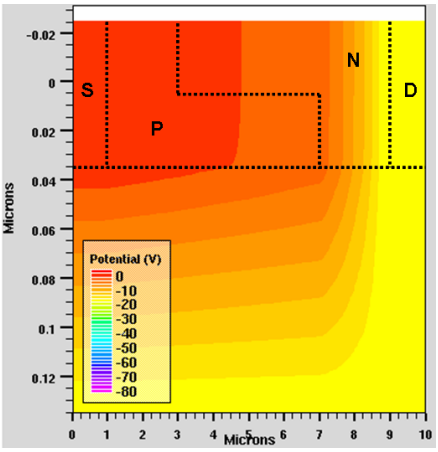

(a) $V_G = -20$ V; $V_D = -20$ V.

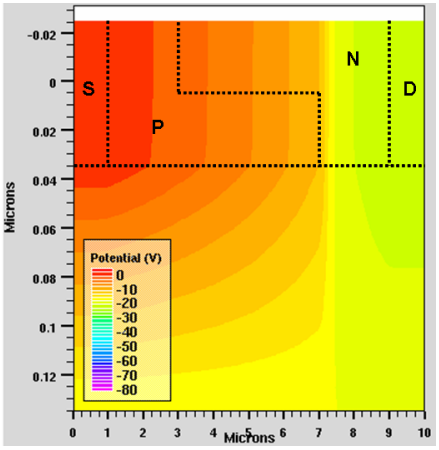

(b) $V_G = -20$ V; $V_D = -25$ V.

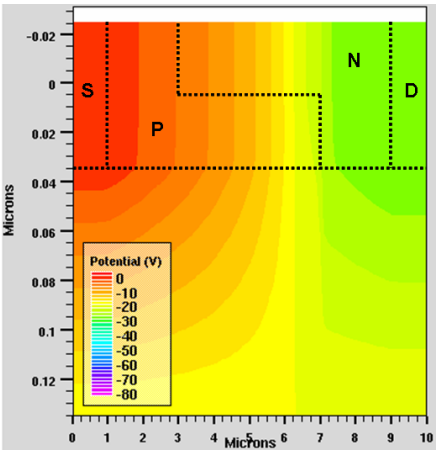

(c) $V_G = -20$ V; $V_D = -30$ V.

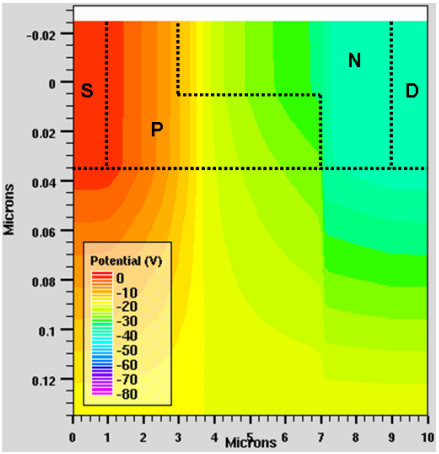

(d) $V_G = -20$ V; $V_D = -40$ V.

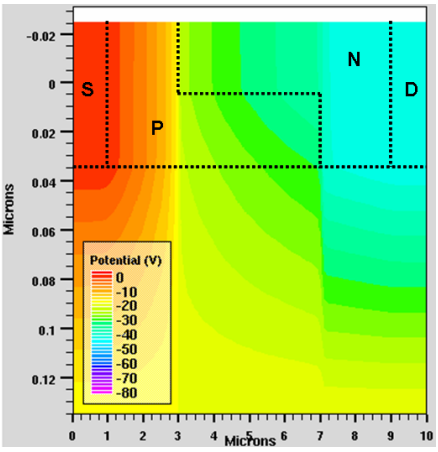

(e) $V_G = -20$ V; $V_D = -45$ V.

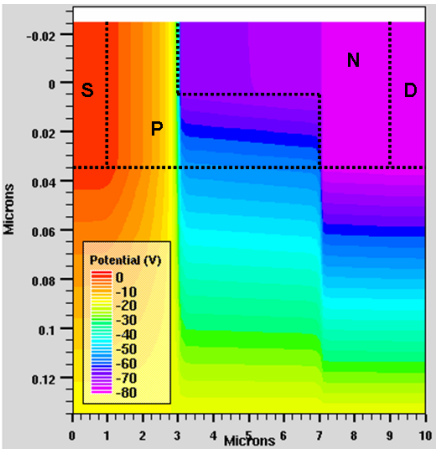

(f) $V_G = -20$ V; $V_D = -80$ V.

Figure 7. Simulated data for the potential in the LEOFET channel.

4. CONCLUSION

In conclusion, we have realized a light-emitting organic field-effect transistor. The device is based on a heterostructure of an n- and a p-type organic semiconductor. The heterostructure is patterned inside the transistor channel by photolithography. The location and the dimensions of the overlapping zone between the two semiconductors can be controlled. This allows for positioning the electron-hole recombination region away from the metal source and drain electrodes. Upon appropriate biasing, we have observed the emission of relatively bright light. Numerical simulations show that the actual recombination region shifts within the transistor channel by changing the biasing conditions, confirming previously published results.

ACKNOWLEDGMENTS

This work is partially supported by the EU-funded Research Projects OLAS (Contract No. 015034), MOLYCELL (Contract No. 502783) and BIOPOLTRONIC (Contract No. 509233). We gratefully acknowledge Sofie Fourier (Hasselt University) for performing the cyclic voltammetry experiments.

REFERENCES

1. H. E. A. Huitema, G. H. Gelinck, J. B. P. H. van der Putten, K. E. Kuijk, K. M. Hart, E. Cantatore and D. M. de Leeuw, "Active-matrix displays driven by solution processed polymeric transistors," *Adv. Mater.* **14**(17), pp. 1201–1204, 2002.
2. G. H. Gelinck, H. E. A. Huitema, E. van Veenendaal, E. Cantatore, L. Schrijnemakers, J. B. P. H. van der Putten, T. C. T. Geuns, M. Beenhakkers, J. B. Giesbers, B.-H. Huisman, E. J. Meijer, E. M. Benito, F. J. Touwslager, A. W. Marsman, B. J. E. Van Rens and D. M. de Leeuw, "Flexible active-matrix displays and shift registers based on solution-processed organic transistors," *Nat. Mater.* **3**(2), pp. 106–110, 2004.
3. M. Kitamura, T. Imada, and Y. Arakawa, "Organic light-emitting diodes driven by pentacene-based thin-film transistors," *Appl. Phys. Lett.* **83**(16), pp. 3410–3412, 2003.
4. A. Hepp, H. Heil, W. Weise, M. Ahles, R. Schmechel, and H. von Seggern, "Light-emitting field-effect transistor based on polycrystalline tetracene," *Phys. Rev. Lett.* **91**(15), p. 157406, 2003.
5. J. Reynaert, D. Cheyns, D. Janssen, R. Müller, V. I. Arkhipov, J. Genoe, G. Borghs, and P. Heremans, "Ambipolar injection in a submicron-channel light-emitting tetracene transistor with distinct source and drain contacts," *J. Appl. Phys.* **97**(11), p. 114501, 2005.
6. C. Santato, R. Capelli, M. A. Loi, M. Murgia, F. Cicoira, V. A. L. Roy, P. Stallinga, R. Zamboni, C. Rost, S. F. Karg, and M. Muccini, "Tetracene-based organic light-emitting transistors: optoelectronic properties and electron injection mechanism," *Synth. Met.* **146**(3), pp. 329–334, 2004.
7. S. Verlaak, D. Cheyns, M. Debucquoy, V. Arkhipov, and P. Heremans, "Numerical simulation of tetracene light-emitting transistors: A detailed balance of exciton processes," *Appl. Phys. Lett.* **85**(12), pp. 2405–2407, 2004.
8. R. Schmechel, A. Hepp, H. Heil, M. Ahles, W. Weise, H. von Seggern, "Light emitting field-effect transistor: simple model and underlying functional mechanisms," *SPIE Proceedings* **5217**, pp. 101–111, 2003.
9. M. Ahles, A. Hepp, R. Schmechel, H. von Seggern, "Light emission from a polymer transistor," *Appl. Phys. Lett.* **84**(3), pp. 428–430, 2004.
10. J. Swensen, D. Moses and A. J. Heeger, "Light emission in the channel region of a polymer thin-film transistor fabricated with gold and aluminum for the source and drain electrodes," *Synth. Met.* **153**(1), pp. 53–56, 2005.
11. T. Oyamada, H. Uchiuzou, S. Akiyama, Y. Oku, N. Shimoji, K. Matsushige, H. Sasabe, and C. Adachi, "Lateral organic light-emitting diode with field-effect transistor characteristics," *J. Appl. Phys.* **98**(7), p. 074506, 2005.
12. A. L. Burin and M. A. Ratner, "Exciton migration and cathode quenching in organic light emitting diodes," *J. Phys. Chem. A* **104**(20), pp. 4704–4710, 2000.
13. H. Becker, S. E. Burns, and R. H. Friend, "Effect of metal films on the photoluminescence and electroluminescence of conjugated polymers," *Phys. Rev. B* **56**, pp. 1893–1905, 1997.

14. C. Rost, S. Karg, W. Rieß, M. A. Loi, M. Murgia, and M. Muccini, "Ambipolar light-emitting organic field-effect transistor," *Appl. Phys. Lett.* **85**(9), pp. 1613–1615, 2004.
15. C. Rost, S. Karg, W. Rieß, M. A. Loi, M. Murgia, and M. Muccini, "Light-emitting ambipolar organic heterostructure field-effect transistor," *Synth. Met.* **146**(3), pp. 237–241, 2004.
16. J. Zaumseil, R. H. Friend and H. Sirringhaus, "Spatial control of the recombination zone in an ambipolar light-emitting organic transistor," *Nat. Mater.* **5**, pp. 69–74, 2006.
17. J. S. Swensen, C. Soci, and A. J. Heeger, "Light emission from an ambipolar semiconducting polymer field-effect transistor," *Appl. Phys. Lett.* **87**(25), p. 253511, 2005.
18. R. E. Gill, A. Meetsma, G. Hadziioannou, "Two novel thermotropic liquid crystalline substituted oligo(*p*-phenylene-vinylene)s: Single crystal X-ray determination of an all-*trans* oligomeric PPV," *Adv. Mater.* **8**(3), pp. 212–214, 1996.
19. C. Rost, D. J. Gundlach, S. Karg, and W. Rieß, "Ambipolar organic field-effect transistor based on an organic heterostructure," *J. Appl. Phys.* **95**(10), pp. 5782–5787, 2004.
20. R. Schmechel, M. Ahles, and H. von Seggern, "A pentacene ambipolar transistor: Experiment and theory," *J. Appl. Phys.* **98**(8), p. 084511, 2005.
21. M. S. Wong, Z. H. Li, M. F. Shek, M. Samoc, A. Samoc, and B. Luther-Davies, "Synthesis and third-order nonlinear optical properties of end-functionalized oligo-phenylenevinylenes," *Chem. Mater.* **14**, pp. 2999–3004, 2002.
22. H. Becker, H. Spreitzer, K. Ibrom, and W. Kreuder, "New Insights into the Microstructure of GILCH-Polymerized PPVs," *Macromolecules* **32**(15), pp. 4925–4932, 1999.
23. F. Babudri, G. M. Farinola, L. C. Lopez, M. G. Martinelli, and F. Naso, "A synthetic strategy leading to monodisperse PPV oligomers by coupling reactions of vinyltrimethylsilanes," *J. Org. Chem.* **66**(11), pp. 3878–3885, 2001.
24. A. J. Bard and L. R. Faulkner, *Electrochemical Methods, Fundamentals and Applications*, Wiley & Sons (New York), 2nd ed. 2001.
25. H. Reiss and A. Heller, "The absolute potential of the standard hydrogen electrode: a new estimate," *J. Phys. Chem.* **89**, pp. 4207–4213, 1985.

APPENDIX A. SYNTHESIS AND ANALYSIS OF OOCTYL-OPV5

The synthesis of OOctyl-OPV5 is depicted in Fig. 8. Firstly, diethyl benzyl phosphonate (**1**) and 4-(diethoxymethyl)-benzaldehyde (**2**) were coupled via a Wadsworth-Emmons reaction in 1,2-dimethoxyethane (DME) using conditions described by Wong *et al*.[21] Subsequent acid deprotection in a two-phase system consisting of 1 M HCl (aq) and diethyl ether afforded *trans*-4-stilbenecarboxaldehyde (**3**) in 85% yield. Secondly, 1,4-bis(octyloxy)benzene (**4**) was reacted with paraformaldehyde and HCl using conditions described by Becker[22] to give **5** in 97% yield. Heating of **5** with triethyl phosphite afforded the bis(phosphonate) **6** in 97% yield. A second Wadsworth-Emmons coupling of **6** with 2 eq. of **3** in DME afforded OOctyl-OPV5. The product was crystallized twice from MeOH/THF (yield: 44%). The purity of OOctyl-OPV5 was established with HPLC and the compound was fully characterised by melting point, ^{1}H NMR, ^{13}C NMR, FT-IR, absorption and fluorescence spectroscopy. These data (not given) were in agreement with literature data.[18,23]

Cyclic voltammetry was performed with an Eco Chemie Autolab PGSTAT 20 Potentiostat/Galvanostat using a conventional three-electrode cell (electrolyte: 0.1 M $TBAPF_6$ in anhydrous CH_3CN) with an Ag/Ag^+ reference electrode (0.01 M $AgNO_3$, 0.1 M $TBAPF_6$ in CH_3CN), a Pt counter electrode and a Pt disk (2 mm diameter) as working electrode. OOctyl-OPV5 was drop casted from a $CHCl_3$ solution onto the Pt working electrode. Cyclic voltammograms were recorded at 50 mV s^{-1} under N_2 atmosphere. All potentials were referenced to the ferrocene/ferrocinium couple (Cp_2Fe/Cp_2Fe^+) which was regularly measured internally. For conversion to eV, we used an estimated value for $E^0(Cp_2Fe/Cp_2Fe^+)$ in CH_3CN of –4.98 V versus the vacuum energy level[24,25] *.

*For the Cp_2Fe/Cp_2Fe^+ couple, we measure a value of 0.06 V versus $Ag/AgNO_3$ in CH_3CN. The Cp_2Fe/Cp_2Fe^+ couple in CH_3CN has a potential of 0.31 V versus aqueous SCE,[24] and the latter has a potential of 0.242 V versus the standard hydrogen electrode (NHE).[24] Since NHE has a potential of –4.43 V versus vacuum,[25] we arrive at a value of –4.98 V versus vacuum for the Cp_2Fe/Cp_2Fe^+ couple in CH_3CN.

The HOMO and LUMO levels were taken as the onset (intersection of baseline and tangent at the inflection point) of the oxidation and reduction waves, respectively, as shown in Fig. 9. The extracted values for the HOMO and LUMO are 5.49 eV and 2.9 eV, respectively (average of three independent measurements).

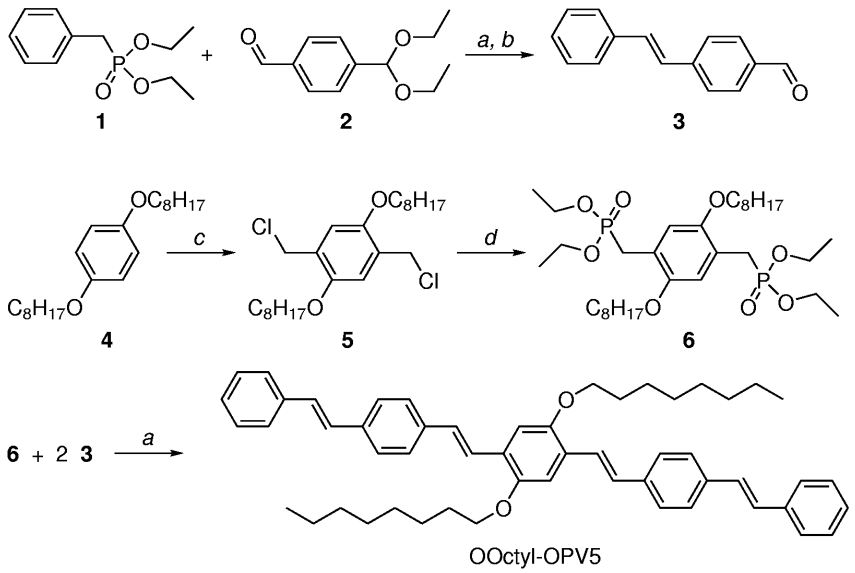

Figure 8. Synthetic route towards OOctyl-OPV5. Conditions: *a)* NaH, DME, 0—20°C; *b)* 1 M HCl, diethyl ether, 20 h; *c)* 37% HCl, paraformaldehyde, acetic acid anhydride, 90°C; *d)* triethyl phosphite, 150—180°C, 2 h.

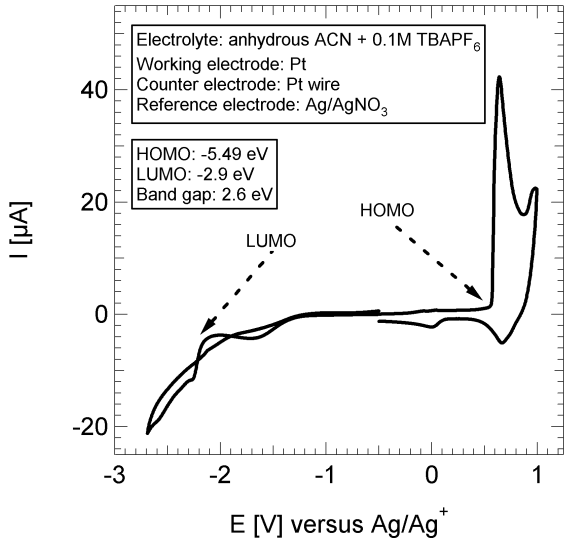

Figure 9. Cyclic voltammogram of OOctyl-OPV5. The measured values for the HOMO and LUMO are 5.49 eV and 2.9 eV, respectively.